Available online at www.sciencedirect.com
SCIENCE DIRECT
Journal of Molecular Catalysis A: Chemical 245 (2006) 114–121
JOURNAL OF MOLECULAR CATALYSIS A: CHEMICAL
www.elsevier.com/locate/molcata

# Electrocatalytic properties of electrodeposited Ni–15Mo cathodes for the HER in acid solutions: Synergistic electronic effect

S. Martinez, M. Metikoš-Huković *, L. Valek

*University of Zagreb, Faculty of Chemical Engineering and Technology, Department of Electrochemistry, Marulićev Trg 19, P.O. Box 177, HR-10002 Zagreb, Croatia*

Received 9 September 2005; received in revised form 26 September 2005; accepted 26 September 2005
Available online 2 November 2005

**Abstract**

The electrocatalytic evolution of $H_2$ in acid solution on well-adhering layers of Ni and Ni–Mo alloy (15 at.% Mo) electrodeposited from a citrate bath onto a glassy carbon disc has been investigated. The kinetic parameters and the rate constants of the forward and backward reactions of Volmer, Heyrovsky and Tafel steps for the hydrogen evolution reaction (HER) were deduced from the linear polarization and electrochemical impedance spectroscopy (EIS) measurements. The high apparent catalytic activity was interpreted with a porous structure of the Ni–15Mo deposits having an enlarged number of active sites.

The main factor influencing outstandingly high electrocatalytic activity of the Ni–15Mo electrodes as a cathode material in terms of HER in acid media has been explained by the synergistic electronic effects. The synergy was interpreted with theoretical predictions based on the complex band structure calculations and magnetic properties of Ni–Mo which suggest a pronounced density of states in d orbitals at the Fermi level obtained by alloying Ni with the threshold content of paramagnetic Mo.

The enhanced catalytic activity of the Ni–15Mo catalyst in comparison with the Ni catalyst in an acid solution was discussed within the framework of a bifunctional Volmer–Heyrovsky mechanism in which the simple cooperative functioning of the alloy components is mediated via a rapid intra-(inter) H-adatoms diffusion. Ni-sites act as an H-source for Mo-sites where the ion-atom recombination (and $H_2$ desorption) takes place. As a results, the ion-atom recombination reaction rate increases in comparison to pure Ni.


*Keywords:* Electrocatalysis; Ni–15Mo catalyst; Hydrogen evolution; Synergistic effect; Electrodeposition

## 1. Introduction

Ni-based alloys display a high electrocatalytic activity for hydrogen evolution in alkaline media [1–8], while little attention has been paid to this phenomenon in acidic media [9–12], in spite of the good prospects of stabilization towards corrosion by the addition of elements such as Cu, Cr, P, Nb and W [12].

The growing interest in commercial application of solid polymer electrolyte membrane (PEM)-type generators has stimulated the study of Ni-based materials as cheaper alternatives to Pt and Ir electrodes to lower investment costs. It has been established that alloying Ni with Mo enhances the electrocatalytic activity of bare nickel [1,9,10,13]. A few theoretical statements have been used to predict the electrocatalytic properties of the *hypo-hyper-d* alloys and their intermetallics [14–16]. A simple mechanism for the increasing hydrogen evolution reaction activity of the *hypo-hyper-d* alloys based on the Brewer–Engel valence-bond theory is frequently cited in literature [14,15]. A somewhat different view results from the tight-binding linear muffin-tin-orbital atomic sphere approximation method [17,18] in combination with magnetization measurements [19–23], that has been successfully applied to rare earth and transition metals and, in particular, to some alloys of special interest for the HER [17]. A more sophisticated mathematical refinement, based upon modern physical approaches providing more reliable estimates, has revealed a more complex mechanism than that predicted by the Brewer–Engel theory. This indicates that the increase in electrochemical activity should be ascribed to an

* Corresponding author. Tel.: +385 1 4597 140; fax: +385 1 4597 139.
*E-mail addresses:* mmetik@marie.fkit.hr, mmetik@fkit.hr (M. Metikoš-Huković).

1381-1169/$ – see front matter © 2005 Elsevier B.V. All rights reserved.
doi:10.1016/j.molcata.2005.09.040

**Nomenclature**

| | |
|---|---|
| $A$ | electrode surface area ($m^2$) |
| $b$ | Tafel slope ($V\,dec^{-1}$) |
| $c$ | concentration ($mol\,m^{-3}$) |
| $C$ | capacitance ($F\,m^{-2}$) |
| CPE | constant phase element |
| $D$ | diffusion coefficient ($m^2\,s^{-1}$) |
| $E$ | potential (V) |
| $F$ | Faraday constant ($96\,485\,C\,mol^{-1}$) |
| $j$ | current density ($A\,m^{-2}$) |
| $k$ | reaction rate constant ($mol\,m^{-2}\,s^{-1}$) |
| $l$ | pore length (m) |
| $n$ | characteristic parameter of CPE |
| $n$ | number of pores |
| $r$ | radius of pores (m) |
| $R$ | resistance ($\Omega\,m^2$) |
| $R$ | gas constant ($8.314\,J\,mol^{-1}\,K^{-1}$) |
| $T$ | absolute temperature (K) |
| $v$ | reaction rate ($mol\,m^{-2}\,s^{-2}$) |
| $z$ | number of electrons |
| $Z$ | impedance ($\Omega\,m^2$) |

*Greek letters*

| | |
|---|---|
| $\eta$ | overpotential (V) |
| $\theta$ | phase angle (°) |
| $\rho$ | electrolyte resistance ($\Omega\,m$) |
| $\upsilon$ | parameter describing the relation between the potential and concentration gradient (V) |

*Subscripts*

| | |
|---|---|
| abs | absorbed |
| ads | adsorbed |
| c | cathodic |
| ct | charge transfer |
| dl | double layer |
| el | electrolyte |
| oc | open circuit |
| $\Omega$ | ohmic |

overall modification of the density of states of the host metal rather than to electron transfer.

Modification of the electronic structure of ferromagnetic Ni alloyed with paramagnetic Mo is indicated by a nonlinear decrease in magnetization with increasing Mo concentration [19]. The ferromagnetic ordering vanishes around 8 at.% (≈12 wt.%) Mo indicating that the simple picture of a linear decrease in the magnetic moment does not hold. It was found [5,9,10] that maximum electrocatalytic activity and the optimum performance of Ni–Mo(W) catalysts toward the hydrogen evolution reaction can be obtained by utilizing a threshold concentration of Mo(W) (≤15 at.%) alloyed with Ni. This result can be explained as a pronounced synergy between Ni, which has internally paired d electrons ($3d^8$), and Mo(W), which has half-filled d orbital ($4d^5$) and therefore can bind hydrogen atoms strongly. The activity maximum appears to be related to the point at which the magnetic moment disappears, due to modification of the Ni electronic configuration or, in the simple picture, filling of the d orbital of Ni.

Our aim was to produce well-adhering Ni and Ni–15Mo electrodeposited layers on an inert glassy carbon substrate and to investigate their electrocatalytic activity for the HER in 0.5 M $H_2SO_4$. Choice of electrodeposition variables, such as nucleation of new grains is favoured over the growth of the existing grains [24], leads to high surfaces area electrodes. As Ni–Mo deposits cannot be obtained on a substrate into which significant hydrogen diffusion occurs [25,26], electrodeposition on an inert conducting glassy carbon (GC) substrate was considered.

For metal electrodes in acidic solution the HER occurs via the following well-known reaction steps [1]:

$$M + H_3O^+ + e \underset{k_{-1}}{\overset{k_1}{\Leftrightarrow}} MH_{ads} + H_2O \quad (\text{rate } v_1) \tag{1}$$

$$MH_{ads} + H_3O^+ + e \underset{k_{-2}}{\overset{k_2}{\Leftrightarrow}} H_2 + M + H_2O \quad (\text{rate } v_2) \tag{2}$$

$$MH_{ads} + MH_{ads} \underset{k_{-3}}{\overset{k_3}{\Leftrightarrow}} H_2 + 2M \quad (\text{rate } v_3) \tag{3}$$

Steps (2) or (3) are alternative desorption steps for $H_2$ formation but each follows step (1). The distinction between (1), (2) and (3) as rate-determining steps in the HER is usually accomplished from Tafel slopes or by calculating the rate constants of the forward and backward reactions through simultaneous fitting of polarization and impedance data [1,2,27,28].

## 2. Experimental

The electrocatalytic performance of well adhering electrodeposits of Ni–15Mo and Ni on glassy carbon (GC), compare to a spectrographically pure nickel electrode were investigated for the HER in 0.5 M $H_2SO_4$ solution. Ni and Ni–15Mo films were deposited on a disk-shaped glassy carbon electrode (Sigradur-Sigri Elektrographite, GmbH, Germany) of surface area 0.28 $cm^2$. Before electrodeposition, the GC disc was polished mechanically using 1200 grit emery paper and rinsed with deionised water in an ultrasonic bath. The surface of the GC was activated for electrodeposition by potentiostatic anodic polarization for 25 s in 0.5 M $H_2SO_4$ solution at 3.2 V versus Ag/AgCl electrode [29].

The freshly prepared GC disk was immersed in the plating solution and deposition was carried out at a constant current density of $-70\,mA\,cm^{-2}$ for 1 min. The temperature of Ni plating bath (pH 3.4) was 55 °C and the plating solution composition was: $300\,g\,dm^{-3}$ $NiSO_4{\cdot}6H_2O$, $50\,g\,dm^{-3}$ $NiCl_2{\cdot}6H_2O$, $40\,g\,dm^{-3}$ $H_3BO_3$, $1\,g\,dm^{-3}$ $Na_3C_{12}H_{25}SO_4{\cdot}2H_2O$ (sodium lauryl sulphate). The plating solution composition for Ni–15Mo was: $79\,g\,dm^{-3}$ $NiSO_4{\cdot}6H_2O$, $48\,g\,dm^{-3}$ $Na_2MoO_4{\cdot}2H_2O$, $88\,g\,dm^{-3}$ $Na_3C_6H_5O_7{\cdot}2H_2O$ (tri-sodium citrate 2-hydrate), excess $NH_4OH$, pH 10.5 [6]. A general agreement is that electrodeposition of Ni–Mo films occurs in two steps with the formation of a molybdenum–nickel oxide that is further reduced by hydrogen to a metallic molybdenum–nickel alloy. The surface morphology of the deposited layers was examined using a

Philips XL 30 scanning electron microscope. The composition of the Ni–Mo co-deposit was determined by quantitative energy dispersive X-ray spectrometry (EDAX) attached to the SEM.

All the HER experiments were made at 298 K in de-aerated 0.5 M $H_2SO_4$ aqueous solution (pH = 0.4), using quasi-potentiostatic polarization and ac impedance spectroscopy techniques. Both dc polarization and ac impedance measurements were carried out with a Solartron model 1287 electrochemical interface and a Solartron model 1255 frequency response analyser, controlled by a PC. A standard three-electrode cell was utilized in all measurements. Pt foil was used as a counter electrode and the reference electrode was Ag/AgCl; 3 M KCl. The solution was de-aerated by continuous bubbling with purified nitrogen. Prior to HER measurements, the freshly polished electrode of spectrographically pure Ni ($A = 0.90\ cm^2$) was activated by a cathodic current density of $-100\ mA\ cm^{-2}$ for 20 min. Ed. Ni and Ni–15Mo electrodes were activated by cathodic polarization at −0.65 V versus Ag/AgCl for 5 min. To investigate the kinetics of HER, linear polarization curves were obtained by sweeping the electrode potential from the open circuit potential, $E_{oc} \approx -0.2$ to −0.65 V versus Ag/AgCl for Ni electrodes and from $E_{oc} \approx -0.15$ to −0.45 V versus Ag/AgCl for the Ni–15Mo electrode, at a scan rate of $1\ mV\ s^{-1}$. The Tafel polarization curves were corrected for *IR* drop effects. The uncompensated solution resistance values were determined from ac impedance measurements. Impedance was measured at dc potentials selected mainly in the linear part of the Tafel polarization curves. A small ac voltage with amplitude of 5 mV and a frequency from $10^5$ to $2 \times 10^{-2}$ Hz was superimposed on the applied potential.

## 3. Results and discussion

### 3.1. The composition and surface morphology of the deposited layers

The composition and atomic ratio of the Ni–Mo composite layer were determined by EDAX measurements. The Ni–Mo layer contained ≈78 wt.% Ni and ≈22 wt.% Mo, corresponding to ≈85 at.% Ni and ≈15 at.% Mo. The surface morphology of the deposited layers was analysed by SEM. Both Ni and Ni–15Mo layers exhibit a very rough surface and are composed of approximately spherical particles of relatively uniform micron or submicron sizes (Fig. 1). The Ni–15Mo composite layer surface appears more developed than the Ni layer, and has better granular structure. More pores can be observed on the Ni–15Mo layer. The porosity of the surface layer contributes substantially to the enlargement of the electrode real (effective) surface area and to the number of catalytically active sites.

### 3.2. Polarization measurements

The rate of hydrogen evolution on polycrystalline Ni, electrodeposited Ni and electrodeposited Ni–15Mo electrodes was studied in a 0.5 M $H_2SO_4$ solution by recording quasi-steady-state polarization curves. HER kinetic parameters were determined from linear plots which exhibit Tafel characteristics (Fig. 2). The apparent exchange current densities, $j_0$ that were

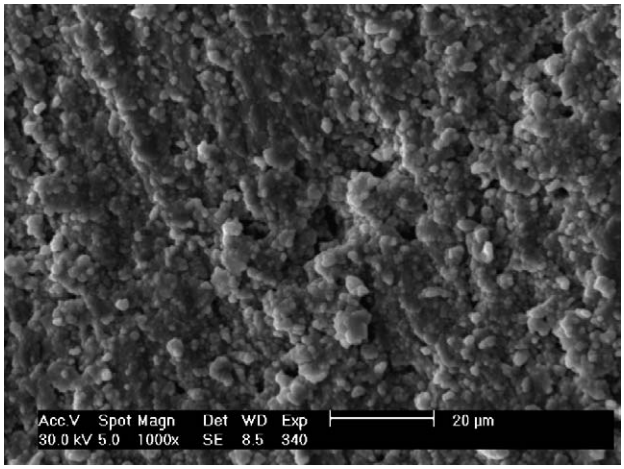


Fig. 1. SEM micrograph of the Ni–15Mo deposit with an original magnification 1000×.

Table 1
Kinetic parameters of the HER obtained from polarization measurements on the polycrystalline Ni, ed. Ni and Ni–15Mo electrodes, in 0.5 M $H_2SO_4$, at 298 K

| | Polycrystalline Ni | Ed. Ni | Ni–15Mo | |
|---|---|---|---|---|
| $b_c$ ($V\ dec^{-1}$) | 0.126 | 0.178 | 0.050 | 0.138 |
| $j_0$ ($A\ cm^{-2}$) | $1.67 \times 10^{-5}$ | $3.1 \times 10^{-4}$ | $3.63 \times 10^{-3}$ | |

estimated by extrapolating the Tafel line to zero overpotential, and the Tafel slopes are listed in Table 1.

Two Tafel regions can be distinguished on the Ni–15Mo polarization curve, with Tafel slopes close to the theoretical values of 40 mV at low overpotentials and 120 mV at high overpotentials, indicating that the Volmer–Heyrovsky mechanism is operative [1]. In the case of ed. Ni, the high values of the Tafel slopes for the Volmer proton discharge step (1), can be explained by the influence of absorbed hydrogen.

Comparison of the kinetic parameters presented in Table 1 for the HER in 0.5 M $H_2SO_4$ solution indicates that, for the ed. Ni electrode, the apparent HER exchange current density, $j_0$, is more than one, and for the Ni–15Mo electrode, more than two orders of magnitude higher than that for polycrystalline Ni. The

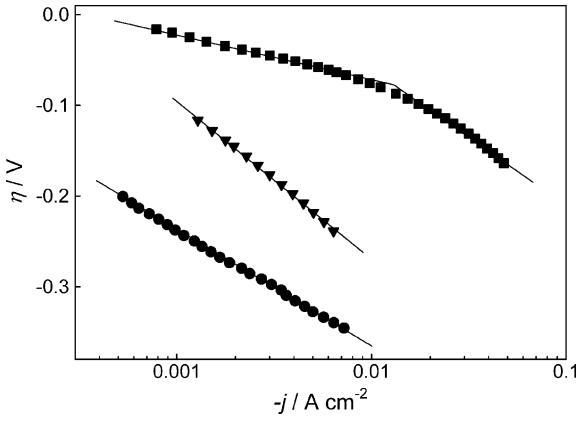


Fig. 2. Quasi-potentiostatic cathodic polarization curves for polycrystalline Ni (●), ed. Ni (▼) and Ni–15Mo (■) electrodes in 0.5 M $H_2SO_4$.

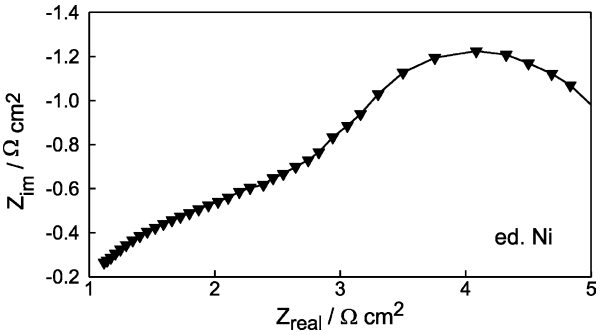


Fig. 3. Complex plane impedance spectrum of the ed. Ni electrode at the overpotential of −0.367 V in 0.5 M $H_2SO_4$, experimental data (symbols) and calculated data (solid line) obtained using the CNLLS fit to an EEC shown in Fig. 5.

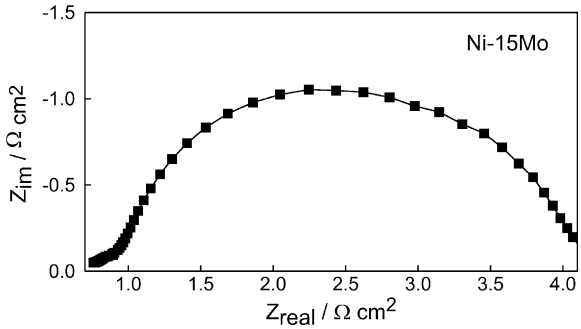


Fig. 4. Complex plane impedance spectrum of the Ni–15Mo electrode at the overpotential of –0.067 V in 0.5 M $H_2SO_4$; experimental data (symbols) and calculated data (solid line) obtained using the CNLLS fit to an EEC shown in Fig. 5.

apparent electrocatalytic activities were almost identical to those obtained by Ezaki et al. [10] on Ni and Ni–Mo (10 at.% Mo) electrodes produced from ultra-fine metal particles and comparable to that for polycrystalline bulk platinum [31–33] in the same solution. Improvements in catalytic activity can generally be achieved through either an increase in the intrinsic activity or an increase in surface area. In comparing different electrode materials (catalysts), it is important to know to what extent the improvements are due to intrinsic changes of electrocatalytic activity (on account of fine particle structure) or simply due to large "scaling factor" values. A qualitative evaluation of the surface morphology of investigated electrodes has shown similar surface roughness of Ni and Ni–15Mo deposits that is significantly higher than that of polycrystalline Ni. Thus, increased performance for $H_2$ evolution on electrodeposited electrodes can be accounted for in terms of the high surface area. Additionally, in case of Ni–15Mo electrode, the synergistic electronic effects between Ni-sites and Mo-sites during this process should be considered.

Although the corrosion properties of Ni and Ni–Mo alloy were not studied in the paper, the following should be mentioned. It is known that Ni dissolves (corrodes) in acid medium. However, under cathodic polarization the dissolution of Ni is negligible and accordingly it could not make any influence on the cathodic currents corresponding to the hydrogen evolution. By alloying Ni with Mo, the corrosion stability of alloy increases. This stabilizing effect is manifested in the change of corrosion potential which is shifted for about 50 mV in comparison to pure Ni.

### *3.3. Electrochemical impedance spectroscopy measurements*

EIS measurements were carried out on ed. Ni and Ni–15Mo electrodes in the range of potentials in which quasi-steady-state polarization curves were recorded. The complex plane impedance diagrams – Nyquist plots presented in Figs. 3 and 4 – suggest porosity of the electrode surfaces. Typically, Nyquist plots of porous electrodes show either a line with a slope of 45° or a semicircle at high frequencies (HF) followed by a semicircle at low frequencies (LF) [28,34–36]. The two constant phase element (2CPE) model introduced by Chen and Lasia [37] has been used to explain the impedance results of Ni and Ni–15Mo electrodeposits. In general, the CPE describes the capacitive semicircle rotated around its centre below the real axes by a frequency independent constant phase angle $\phi = (1 - n)\pi/2$. For a perfect capacitor, $\phi = 0$ ($n = 1$), for a perfect resistor, $\phi = \pi/2$ ($n = 0$) while a value of $\phi = \pi/4$ ($n = 0.5$) points to a diffusion-like phenomenon. $n$ is the exponent of the CPE describing all kinds of inhomogeneity, i.e. physical, chemical and geometrical.

The impedance data of the HER on the ed. Ni electrode were interpreted using the equivalent electric circuit (EEC) for porous electrodes [37] presented in Fig. 5 consisting of a serial connection of two parallel CPE-$R$ circuit elements: $R_{el}((R_1\text{CPE}_1)(R_2\text{CPE}_2))$. Application of the model results in two semicircles. The HF semicircle $\text{CPE}_1$-$R_1$, which is potential independent, is related to the surface porosity and the LF semicircle $\text{CPE}_2$-$R_2$, potential dependent, is related to the kinetics of the Faradaic reaction of the HER.

In the whole overpotential range, the very low resistance $R_1$ and values of the $\text{CPE}_1$ exponent $n_1$ between 0.4 and 0.5 can be related to the ohmic, electrolyte resistance (so called "pore resistance") and diffusion or migration processes in the pores of Ni deposit at the Ni/electrolyte interface, respectively the $\text{CPE}_2$ exponent $n_2$ acquires values between 0.9 and 1. Thus, $\text{CPE}_2$ corresponds to the total interfacial capacitance made up of the double layer capacitance, $C_{dl}$ and pseudocapacitance, $C_\phi$, since $C_{dl}$ was not distinguishable from an adsorption capacitance. $R_2$

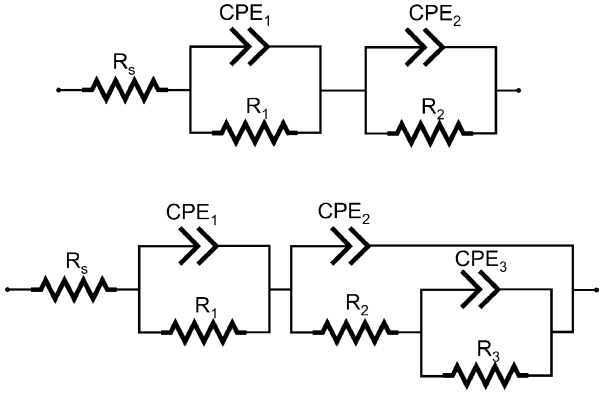


Fig. 5. Equivalent electrical circuits used for fitting EIS experimental data shown in Figs. 3 and 4.

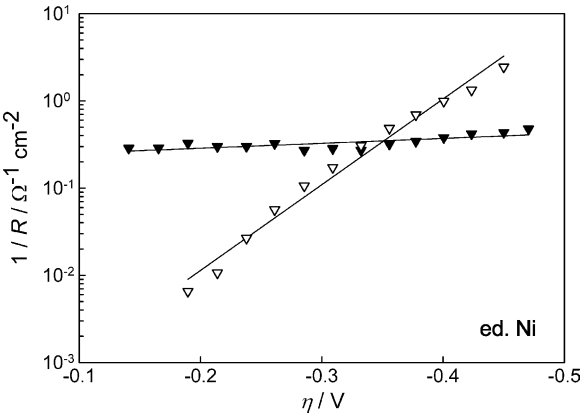


Fig. 6. Dependence of HF (▼) and LF (▽) $\log R^{-1}$ on the overpotential for the ed. Ni electrode in 0.5 M $H_2SO_4$.

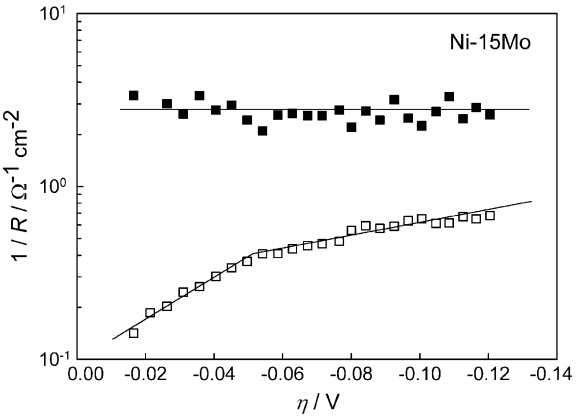


Fig. 7. Dependence of HF (■) and LF (□) $\log R^{-1}$ on the overpotential for the Ni–15Mo electrode in 0.5 M $H_2SO_4$.

corresponds to the charge transfer resistance, $R_{ct}$. Dependence of the pore resistance, $R_1$ and the charge transfer resistance, $R_2$ ($R_{ct}$) on overpotential $\eta$ is shown in Fig. 6. The logarithm of $R_2^{-1}$ ($R_{ct}^{-1}$) depends linearly on the overpotential, while that of $R_1^{-1}$ ($R_\Omega^{-1}$) is essentially constant, substantiating the validity of the porous model. According to the model of de Levie [38], the pore resistivity $R_\Omega = \rho l/n_p \pi r^2$, where $\rho$ is the electrolyte resistance, $l$ the pore length, $n_p$ the number and $r$ the radius. The fact that $R_\Omega^{-1}$ is higher for the Ni–15Mo electrode means that this electrode is more porous than ed. Ni.

The low frequencies part of the 2CPE model for the Ni–15Mo electrode (Fig. 4) has been modified by nesting a $CPE_3$-$R_3$ element in parallel with the $CPE_2$-$R_2$, called Armstrong's EEC. This combination of circuit elements, shown in Fig. 5, has been chosen on the basis of the statistical importance of the newly introduced elements. Error estimates for each circuit element have been calculated using the program developed by Boukamp [39]. It may be assumed that $C_3$ is basically related to the pseudocapacitance, $C_\phi$, of the adsorbed $H_{ads}$ intermediate, and that $R_3$ represents the pseudoresistance related to the mass transfer resistance of the adsorbed $H_{ads}$ intermediate. The Faradaic impedance, $Z_f$ of the low frequency branch of total impedance (Armstrong's EEC) is defined as follows:

$$Z_f = R_2 + \frac{R_3}{1 + j\omega\tau_p}$$

where $\omega$ is the frequency and $\tau_p = R_3C_3$ is the time constant related to the relaxation rate of the adsorbed hydrogen, $H_{ads}$ on the Ni–15Mo electrode when its potential is changed. All parameters are obtained by CNLLS [39] fitting procedure. Values of the impedance parameters obtained for the ed. Ni and Ni–15Mo electrodes were used to interpret the kinetics of HER. At any of selected potentials the sum $(R_2 + R_3)$ presents the total Faradaic resistance of the electrode. Hence, its reciprocal is directly related to the Faradaic current density at the potential considered. Since the HER is charge transfer controlled within the entire region of overpotentials considered, a plot of $\eta$ against $\log(R_2 + R_3)^{-1}$ should be linear and its slope equal to the Tafel slope, $b_c$.

Fig. 7 shows that EIS data give a linear relationship for $\eta$ versus $\log(R_2 + R_3)^{-1}$ with two slopes ($b_{EIS} = -0.75$ mV dec$^{-1}$ and $b_{EIS} = -0.236$ mV), as obtained by quasi-potentiostatic polarization measurements. Based on the validity of the Butler–Volmer equation by utilizing the relation $j_0 = RT(zFR_{ct})^{-1}$, valid for $\eta \to 0$, the exchange current density has been computed. Much higher Tafel slopes ("deactivated values") than the maximum value expected from VH kinetics are believed to be results of in situ hydride formation during a prolonged cathodic polarization by EIS measurements. Very high value of the exchange current density ($j_0 = 2.45 \times 10^{-3}$ A cm$^{-2}$) is obviously caused by the same reason. "Deactivation" is tentatively attributed to the formation of a subsurface hydride. Transition metals with their high density of d states at the Fermi level may undergo drastic changes in their physical properties upon hydrogenation at high overpotentials, without loss of metallic behaviour. In the case of Ni, hydrogen is absorbed interstitially [18,23] acting as an alloy constituent. The presence of the metastable β-phase of Ni hydride under conditions used in this work i.e., during cathodic polarization of Ni in acid solutions, was evident from the in situ XRD measurements [30]. Adsorption of H on Ni involves the d-like bonding component at the Fermi level, $E_F$. The depletion of the d-electron density of state at $E_F$ will tend to suppress further H adsorption. By analogy, absorption of H and formation of a subsurface hydride weakens the adsorptive power of the bare Ni surface and causes "deactivation" of the Ni surface. This could now make proton discharge (step 1) on Ni the rate determining step (RDS) with Tafel slope $b_c \approx 120$ mV dec$^{-1}$.

It is noteworthy that in the case of porous electrodes the rigorous analysis using the potential dependence of $R_{ct}$ is possible only when the pores are identical. In real situations, a distribution of different pore sizes exists [34]. Despite of that, the kinetic parameters obtained from ac impedance measurements are in reasonable agreement with those obtained from the dc polarization studies. Table 1 shows two values for the Tafel slopes, valid respectively at low and intermediate overpotentials. This is because the HER in acid solutions proceeds through two distinct mechanisms (Volmer–Heyrovsky mechanism, steps (1) and (2)). The reaction rates for reactions (1)–(3) can be expressed as

follows:

$$v_1 = k_1(1-\theta)\exp(-\alpha f\eta) - k_{-1}\exp[(1-\alpha)f\eta]$$
$$= k'_1(1-\theta) - k'_{-1}\theta \quad (4)$$

Similarly

$$v_2 = k'_2\theta - k'_{-2}(1-\theta) \quad (5)$$

$$v_3 = k_3\theta^2 - k_{-3}(1-\theta)^2 \quad (6)$$

Here, $k$ are the rate constants, and the symbols + and − denote forward and backward reactions, respectively. $k'$ are constants at a given overpotential. $\theta$ represents the surface coverage by adsorbed hydrogen, $\alpha$ the electron transfer coefficient, and $f = F/RT$. The rate of H adsorption (Eq. (4)) will thus decrease with increasing surface coverage, $\theta$, while the recombination rate of reaction (2) will increase with coverage $\theta$ (Eq. (5)). For this reason, accumulation of H at the metal surface will tend to decrease the effective area still available for H adsorption and slow down this process. With increasing overpotential, the proton discharge reaction (1) will thus become the rate determining step.

By simultaneously fitting the polarization and impedance data in the potential range between −0.017 and −0.13 V, the rate constants of forward and backward reactions were calculated for the Ni–15Mo system by a nonlinear fitting method. Calculated values are: $k_1 = 1.53 \times 10^{-7}$ mol cm$^{-2}$ s$^{-1}$, $k_{-1} = 1.55 \times 10^{-6}$ mol cm$^{-2}$ s$^{-1}$, $k_2 = 8.56 \times 10^{-9}$ mol cm$^{-2}$ s$^{-1}$, $k_{-2} = 8.45 \times 10^{-10}$ mol cm$^{-2}$ s$^{-1}$, $k_3 = 9.27 \times 10^{-8}$ mol cm$^{-2}$ s$^{-1}$, $k_{-3} = 9.03 \times 10^{-10}$ mol cm$^{-2}$ s$^{-1}$. The dependence on potential of the current density ($j$) and the reaction rates of Volmer ($v_1$), Heyrovsky ($v_2$) and Tafel ($v_3$) steps, as well as the corresponding rate constants for the HER on the Ni–15Mo electrode are shown in Fig. 8. The main pathway is Volmer–Heyrovsky, with the rate determining step of Heyrovsky.

For the Ni–15Mo alloy investigated here, Ni is in large excess and its normal functionality is, in any case, out of the question.

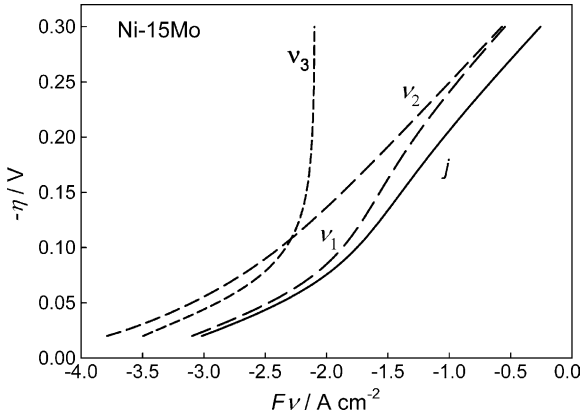


Fig. 8. Potential dependence of the current density and the reaction rates of the HER on the Ni–15Mo electrode. Calculated reaction rates: $k_1 = 1.53 \times 10^{-7}$ mol cm$^{-2}$ s$^{-1}$, $k_{-1} = 1.55 \times 10^{-6}$ mol cm$^{-2}$ s$^{-1}$, $k_2 = 8.56 \times 10^{-9}$ mol cm$^{-2}$ s$^{-1}$, $k_{-2} = 8.45 \times 10^{-10}$ mol cm$^{-2}$ s$^{-1}$, $k_3 = 9.27 \times 10^{-8}$ mol cm$^{-2}$ s$^{-1}$, $k_{-3} = 9.03 \times 10^{-10}$ mol cm$^{-2}$ s$^{-1}$.

Ni also affects the proton discharge step (1) at a significant rate. Unlike Ni, the marginal perturbation of the Fermi level of Mo by adsorbed H may be attributed to its high d character [40]. The mechanistic link responsible for the synergistic effect between Ni and Mo can be described in a bifunctional mechanism framework as follows [9,11]. The hydrogen ions discharged on Ni-sites and adsorbed H-adatoms may further diffuse from Ni to Mo-sites. Due to the strong bonding of H by Mo, there is a high probability for two hydrogen atoms to be bound simultaneously and to recombine there (step (2)). As a result, the rate of ion-atom recombination is greater than that for pure Ni. In this way, the "deactivation" of the electrode by the excessive coverage of adsorbed hydrogen can be reduced by the fast recombination rate achieved on Mo, while the high electrochemical activity of Ni for hydrogen adsorption makes Ni a source of hydrogen for Mo. This synergistic reaction mechanism can be expressed as follows [11]:

$$\text{Ni} + \text{H}^+ + \text{e}^- \leftrightarrow \text{Ni-H}_{\text{ads}} \quad (7)$$

$$\text{Ni-H}_{\text{ads}} + \text{Mo} \leftrightarrow \text{Ni} + \text{Mo-H}_{\text{ads}} \quad (8)$$

$$\text{Mo-H}_{\text{ads}} + \text{H}^+ + \text{e}^- \leftrightarrow \text{H}_2\uparrow + \text{Mo} \quad (9)$$

Thus, H adatoms, created by Ni diffuse, to a neighbouring Mo "trap" centre. The activation energy for surface diffusion is only a small fraction of that required for molecular desorption, and ranges from 10 to 25 kJ mol$^{-1}$ [41]. According to Highfield et al. [9] only a surface dynamic phenomenon like "spillover" can explain the synergy in physical mixtures, in which any statement based on electronic interaction between the components is essentially ruled out. The synergy would be expected to be expressed optimally in the alloys, due to the favourable spatial distribution and atomic dispersion of the constituents.

### 3.4. Porous electrode model

By taking into account the implications of the porous electrode models [34,35,37,38,42,43], some conclusions can be drawn about the process occurring on the investigated electrodes. De Levie's model [38] of the HER on porous electrodes predicts linear behaviour of the HF part of the Nyquist plot and relates it to the resistance-double layer capacitance coupling in the semi-infinite cylindrical pores. De Levie's model does not account for the electrolytic diffusion of species in the pores, but only takes into account the potential drops there. It was originally derived for the case of zero dc current while, in the presence of finite dc current, only the numerical solution, derived by Lasia, exists [34]. The solution derived by Lasia is more general and shows that the shape of the complex impedance plots for the fixed pore dimensions and electrolyte conductivity, in the presence of the potential gradient and the absence of the concentration gradient, depends strongly on the exchange current density, the overpotential and the HER transfer coefficient. In the presence of a concentration gradient in the finite length pores, the HF semicircle is generally observed [35,36], being pronounced at medium overpotentials, for finite-length pores, and at high concentration

of the diffusing species in the bulk. As the penetration depth of the ac signal depends on frequency, the pores respond at low frequencies like a flat electrode, yielding a LF semicircle.

In order to distinguish between the prevailing concentration gradient and the influence of potential drop, the parameter $\upsilon$,

$$\upsilon = nFD_{H_2}c^*_{H_2}\rho \quad (10)$$

can be calculated, where $D_{H_2}$ and $c^*_{H_2}$ are the diffusion coefficient and concentration of $H_2$ species, respectively, $\rho$ is the resistivity of the electrolyte and $F$ is the Faraday constant [35]. For $\upsilon < 1$ the system is determined principally by the concentration gradient, while for $\upsilon > 1$, it is determined by the potential drop in the pores. Taking $D_{H_2} = 7 \times 10^{-5}\,cm^2\,s^{-1}$, $c^*_{H_2} = 8 \times 10^{-8}\,mol\,cm^{-3}$ and $\rho = 4.81\,\Omega\,cm$, Eq. (10) gives $\upsilon = 5.2 \times 10^{-6}$ V. Apparently, no influence of the potential drop is expected for the present system. The somewhat flattened appearance of the HF semicircles shown in Figs. 3 and 4 is therefore not due to the influence of the potential drop in the pores but may originate from the pear shape of the spherical pores, the latter producing flattened semicircles changing to a straight line at larger pore openings [28].

Real area determination, i.e. the determination of roughness factor according to the double layer procedure was not performed due to the following reasons:

(i) this procedure is seriously unreliable unless it has been shown that electrolyte conductivity in the porous matrix is sufficiently high to sustain the double layer capacity measurement without dispersion due to de Levie porous-electrode effect,
(ii) also, for electrocatalytic metals at which $H_2$ is being evolved, the real area determination from capacity measurements is questionable since the double layer capacity is not distinguishable from pseudocapacitance of chemisorbed H intermediate.

## 4. Conclusions

The Ni–15Mo catalyst, designed for the HER, was electrodeposited from a citrate bath on the glassy carbon disc and investigated by polarization and EIS measurements in 0.5 M $H_2SO_4$ solution. Surface composition was tailored according to the magnetization measurements [4] on sputter and electrodeposited Ni–Mo alloy in a dependence of Mo content in the alloy.

Optimum chemical composition of alloys and compounds of transition metals as catalysts, in general, can be related to the highest density of states at the Fermi level and in turn to the maximum synergy effect for the HER. Thus, by producing an alloy as catalyst, with the intention to have excellent catalytic activity for the HER, a "threshold" concentration of the alloying element should be utilized. This concentration can be predicted theoretically by performing a complex electronic calculation or determined experimentally by magnetization measurements.

Kinetic parameters, indicative for electrocatalytic properties of the Ni–Mo (15 at.%) alloy towards the HER were determined from the linear polarization and electrochemical impedance spectroscopy measurements.

The porosity of electrodeposited electrodes is substantiated by the EIS results, to which the 2CPE model has been successfully applied and certain conclusions regarding the occurrence of the HER within the pores drawn. According to this model the HER probably occurs under the influence of a concentration gradient within the finite length pores that differ in size and are of irregular shape.

By simultaneously fitting the polarization and impedance data, the rate constants of the forward and backward reactions for the HER were calculated for the Ni–15Mo system. It was established that $H_2$ evolution over the Ni–15Mo electrode in 0.5 M $H_2SO_4$ solution proceeds via a Volmer–Heyrovsky mechanism. The main factor influencing the performance of Ni–15Mo electrodes as cathode materials toward the HER in acidic media was explained in terms of the synergistic electronic effects. The synergy was interpreted on the basis of modification of the electron density of the states in d orbitals by alloying nickel with "threshold" content of molybdenum. The enhanced catalytic activity of the Ni–15Mo catalyst in comparison with the Ni catalyst has been described within the framework of a Volmer–Heyrovsky mechanism in which "surface dynamics" of intermediate H adatoms occur between Ni – sites and Mo – sites – the well known "spillover" process in heterogeneous catalysis.

## Acknowledgement

The financial support of Ministry of Science (Projects 015 011/014) and EU-INCO Project "Prometheas" (Contract No.: ICA2-CT-2001-10037) is gratefully acknowledged.

## References

[1] J.M. Jakšić, M.V. Vojnović, N.V. Krstajić, Electrochim. Acta 45 (2000) 4151.
[2] A. Lasia, A. Rami, J. Electroanal. Chem. 294 (1990) 123.
[3] M.V. Ananth, N.V. Partasardhy, Int. J. Hydrogen Energy 22 (1997) 747.
[4] M. Metikoš-Huković, A. Jukić, Electrochim. Acta 45 (2000) 4159.
[5] A. Kawashima, E. Akiyama, H. Habazaki, K. Hashimoto, Mater. Sci. Eng. A226–A228 (1997) 905–909.
[6] C. Fan, D.L. Piron, A. Sleb, P. Paradis, J. Electrochem. Soc. 141 (1994) 382.
[7] C. Fan, D.L. Piron, A. Sleb, P. Paradis, J. Electrochem. Soc. 39 (1994) 2715.
[8] C. Fan, D.L. Piron, P. Paradis, Electrochim. Acta 39 (1994) 2715.
[9] J.G. Highfield, E. Claude, K. Oguro, Electrochim. Acta 44 (1999) 2805.
[10] H. Ezaki, T. Nambu, M. Morinaga, M. Udaka, K. Kawasaki, Int. J. Hydrogen Energy 21 (1996) 877.
[11] G. Lu, P. Evans, G. Zangari, J. Electrochem. Soc. 150 (2003) A551.
[12] G. Lu, G. Zangari, Electrochim. Acta 47 (2002) 2969.
[13] C.-C. Hu, C.-Y. Weng, J. Appl. Electrochem. 30 (2000) 499.
[14] M.M. Jaksic, Electrochim. Acta 25 (1984) 1539.
[15] J.M. Jaksic, N.M. Ristic, N.V. Krstajic, M.M. Jaksic, Int. J. Hydrogen Energy 23 (1998) 1121.
[16] J. Ezaki, M. Morinaga, S. Watanabe, Electrochim. Acta 38 (1993) 557.
[17] B. Szpunar, M. Aus, C. Cheung, U. Erb, G. Palumbo, J.A. Szpunar, J. Magn. Magn. Mater. 187 (1998) 325.
[18] M. Hanson, H.J. Bauer, J. Alloys Comp. 179 (1992) 339.
[19] F.A. Khan, M.A. Asgar, P. Nordblad, J. Magn. Magn. Mater. 174 (1997) 121.

[20] M.V. Ananth, N.V. Partasardhy, Mater. Sci. Eng. B5 (1990) 451.
[21] A. Stephen, T. Nagarajan, M.V. Ananth, Mater. Sci. Eng. B55 (1998) 184.
[22] A. Burgstaller, W. Socher, J. Voitländer, I. Bakonyi, E. Tóth-Kádár, A. Lovas, H. Ebert, J. Magn. Magn. Mater. 109 (1992) 117.
[23] S.M. Tavares, S. Miraglia, A. Lafuente, D. Fruchart, J. Magn. Magn. Mater. 242–245 (2002) 898.
[24] U. Erb, Nanostructured Mater. 6 (1995) 533.
[25] J. Crousier, M. Eyraud, J.P. Crousier, J. Appl. Electrochem. 22 (1992) 749.
[26] L. Mirkova, G. Maurin, M. Monev, Chr. Tsvetkova, J. Appl. Electrochem. 33 (2003) 93.
[27] B. Losiewicz, A. Budniok, E. Rowinski, E. Lagiewka, A. Lasia, Int. J. Hydrogen Energy 29 (2004) 145.
[28] A. Hitz, A. Lasia, J. Electroanal. Chem. 500 (2001) 213.
[29] A. Dekanski, Carbon 39 (2001) 1195–1205.
[30] R. Juskenas, A. Selsekis, V. Kadziauskiene, V. Jasulaitiene, Joint Meeting of the Electrochemical Society, Inc., International Society of Electrochemistry, Paris, France, Meeting Abstracts, vol. 97-2, Abb. 933, August 31–September 5, 1997, p. 1071.
[31] S. Trasatti, J. Electroanal. Chem. 39 (1972) 163.
[32] L.I. Krishtalik, in: P. Delahay (Ed.), Advances in Electrochemistry and Electrochemistry Engineering, vol. 7, Interscience, New York, 1970, p. 283.
[33] S. Trasatti, J. Chem. Soc., Faraday Trans. 68 (1972) 229.
[34] A. Lasia, J. Electroanal. Chem. 397 (1995) 27.
[35] A. Lasia, J. Electroanal. Chem. 428 (1997) 155.
[36] A. Lasia, J. Electroanal. Chem. 500 (2000) 30.
[37] L. Chen, A. Lasia, J. Electrochem. Soc. 138 (1991) 3321.
[38] R. de Levie, in: P. Delahay (Ed.), Advances in Electrochemistry and Electrochemistry Engineering, vol. 6, Interscience, New York, 1967, p. 329.
[39] B.A. Boukamp, Solid State Ionics 20 (1980) 31.
[40] J.K. Norskov, F. Besenbacher, J. Less-Common Met. 130 (1987) 475.
[41] K.R. Christmann, in: Z. Paal, P.G. Menon (Eds.), Hydrogen Effects in Catalysis, Marcel Dekker, 1988, p. 3, Chapter 1.
[42] L. Birry, A. Lasia, J. Appl. Electrochem. 34 (2004) 735.
[43] A. Hasbach, U. Retter, K. Siegler, W. Kautek, J. Electroanal. Chem. 561 (2004) 29–35.